



High-Order Bound-Preserving Finite Difference Methods for Incompressible Wormhole Propagation

Xinyuan Liu¹ · Yang Yang² · Hui Guo¹

Received: 24 December 2020 / Revised: 28 June 2021 / Accepted: 4 August 2021

© The Author(s), under exclusive licence to Springer Science+Business Media, LLC, part of Springer Nature 2021

Abstract

In this paper we continue our effort in Guo et al. (J Comput Phys 406:109219, 2020) for developing high-order bound-preserving (BP) finite difference (FD) methods. We will construct high-order BP FD schemes for the incompressible wormhole propagation. Wormhole propagation is used to describe the phenomenon of channel evolution of acid and the increase of porosity in carbonate reservoirs during the acidization of carbonate reservoirs. In wormhole propagation, the important physical properties of acid concentration and porosity involve their boundness between 0 and 1 and the monotonically increasing porosity. High-order BP FD methods can maintain the high-order accuracy and keep these important physical properties, simultaneously. The main idea is to choose a suitable time step size in the BP technique and construct a consistent flux pair between the pressure and concentration equations to deduce a ghost equation. Therefore, we can apply the positivity-preserving technique to the original and the deduced equations. Moreover, the high-order accuracy is attained by the parametrized flux limiter. Numerical experiments are presented to verify the high-order accuracy and effectiveness of the given scheme.

Keywords Incompressible wormhole propagation · Bound-preserving · High-order · Finite difference method · Flux limiter

Mathematics Subject Classifications (2000) 65M15 · 65M60

The first author was supported by Graduate Innovation Projects grant YCX2020114. The second author was supported by NSF grant DMS-1818467. The last author was supported by the Fundamental Research Funds for the Central Universities 20CX05011A.

✉ Hui Guo
sdugh@163.com

Xinyuan Liu
s18090001@s.upc.edu.cn

Yang Yang
yyang7@mtu.edu

¹ College of Science, China University of Petroleum, Qingdao 266580, China

² Department of Mathematical Sciences, Michigan Technological University, Houghton, MI 49931, USA

1 Introduction

Acidization, as a stimulation technique, has been commonly used to increase the production of petroleum reservoirs. In this technique, acid is injected into wells to dissolve the material near and/or in the wellbore, which can increase the permeability and porosity of the material close to a well. Therefore, under optimal injection rate, the rapid rates of dissolution and heterogeneous flow profiles lead to the formation of highly conductive flow channels, commonly referred to as wormholes. Wormholes can establish a good connectivity between the reservoir and the wellbore, thereby greatly improving the productivity of the oil well. Due to the significant role that wormhole plays in subsurface reservoir management, there are many research works have been done on the formation and propagation of wormholes.

The earliest research of wormhole propagation phenomenon was carried out through experiments in [7,14]. With the establishment of mathematical models such as dimensionless model, capillary model, network model, and continuum model, people had a better understanding of wormhole propagation process. In [22], Panga et al. developed the two-scale continuum model and proposed a partial differential equations system to describe the formation and propagation of wormholes. Based on this model, there were many follow-up works. Zhao et al. [33] presented the theoretical and numerical analysis on the front instability of wormhole propagation. 3D simulation of carbonate acidization was presented by Maheshwari et al. in [21]. In [28], Wu et al. conducted a parallel simulation under a modification of flow equation. In 2017, the authors in [1] studied the numerical-simulation approach for a modified model. Later, Wei et al. [27] extended this model from single phase flow to two-phase flow. In addition to the above works, many researchers also designed specific numerical schemes for this model. In [17], Sun et al. proposed a fully conservative method based on mixed finite element to simulate the wormhole propagation. Later, Li and Rui [18,19] applied finite difference (FD) methods to this problem. Moreover, in [12], Guo et al. applied the discontinuous Galerkin (DG) method to this model.

It is well known that the exact solutions of incompressible wormhole prorogations satisfy some physical bounds, e.g. the concentration of acid c_f is between 0 and 1, and the porosity ϕ is increasing during time evolution and less than 1. In many numerical simulations, the numerical approximations of c_f may be placed outside the bounds, especially if the exact solution contains discontinuities or large gradients. Moreover, the time derivative of ϕ depends on c_f , and the negative approximations of c_f can further lead to $\phi < 0$ in some regions with low porosity. In addition, near the wormhole, the numerical oscillations of ϕ itself may also cause negative values. Both of the above two cases will bring a negative coefficient in the diffusion term of the transport equation. Numerical experiments in [31] have demonstrated that if the numerical approximations are out of the physical bounds, the problems can be ill-posed, leading to the instability of numerical simulations. Thus, the bound-preserving (BP) technique is essential for numerical simulations.

The BP technique for fractions was recently introduced in [13], where two of the authors in the present study applied second-order DG methods for compressible miscible displacements in porous media. Subsequently, the high-order extension on unstructured triangular meshes was discussed in [3]. Later, the authors further investigated high-order BP DG methods for multispecies and multireaction detonations [5,6] and incompressible wormhole propagations [31]. One of the key steps in the numerical algorithm is to apply the “consistent” numerical flux (see Definition 3.1). However, the ideas introduced in the works given above are not straightforward extendable to FD schemes. In fact, the BP technique for FD methods was mainly based on flux limiters, and it was first introduced in [30], where the maximum-

principle-preserving FD methods were investigated for hyperbolic equations in one space dimension. The extension to convection-diffusion equations was given in [16,29]. The basic idea is to modify the numerical fluxes by combining the first-order and high-order numerical fluxes. Therefore, the time step size has to be predetermined before the usage of the flux limiters. In [11], the authors demonstrated that direct usage of the BP technique in [3,13,31] can result in time step size paradox. This is mainly due to the fact that the requirement of “consistent” numerical flux in the BP technique will result in a new time step size requirement for the source term after the application of flux limiters. To fix this gap, in [11], we used the same stencil to construct the high-order and first-order numerical fluxes and developed high-order BP FD methods for miscible displacements in porous media. However, to the best knowledge of the authors, no previous works discussing the high-order BP FD methods for incompressible wormhole propagation are available. In this paper, we will establish high-order BP FD schemes in this direction and keep the bounds of concentration of acid and porosity. For the incompressible wormhole propagation, since the initial values of Darcy’s velocity \mathbf{u} and pressure p are not given, we need to solve a large system of linear equations at each time level to obtain numerical approximations of these two variables. As a result, unlike [11], we need to construct a special numerical flux for the pressure equation to be “consistent” with that for the concentration equation to obtain a ghost equation satisfied by $c_2 = 1 - c_f$. Then we apply the positivity-preserving technique can be applied on both the original and ghost equations. Moreover, different from miscible displacements in porous media, the porosity ϕ in wormhole propagation is bounded between 0 and 1, and it is increasing during time evolution. Therefore, we also need to preserve the positivity of ϕ_t to obtain physically relevant ϕ . To construct the BP technique, we define a new variable $r = \phi c_f$, and then apply the positivity-preserving flux limiter to r instead of c_f . Therefore, the upper bound of r , say ϕ , is changing during time evolution. We introduce special techniques to obtain physically relevant ϕ . In summary, the whole algorithm can be divided into three parts. Firstly, We apply positivity-preserving technique to obtain positive ϕ_t and use which in pressure equation to seek the velocity and pressure. Then apply the positivity-preserving (PP) technique again to c_f and $1 - \phi$ simultaneously to obtain physically relevant numerical approximations. Finally, we use “consistent” flux pair in the flux limiter in both the concentration and pressure equations to obtain the positive approximation of $1 - c_f$, which further yields physically relevant numerical approximations of c_f .

The rest of the paper is organized as follows: we first introduce the mathematical model of the incompressible wormhole propagation in Sect. 2. In Sect. 3, we construct the FD scheme in two space dimensions. We demonstrate the BP technique for both first-order and high-order schemes in Sect. 4. In Sect. 5, some numerical experiments will be carried out to verify the high-order accuracy and effectiveness of the numerical technique. Finally, concluding remarks are given in Sect. 6.

2 Mathematical Model

In this section, we introduce the mathematical model of the incompressible wormhole propagation. Let $\Omega = [0, 2\pi] \times [0, 2\pi]$ and $J = [0, T]$, the mathematical model of the incompressible wormhole propagation is as follows:

$$\frac{\partial \phi}{\partial t} + \nabla \cdot \mathbf{u} = f, \quad (x, y) \in \Omega, \quad 0 < t \leq T, \tag{2.1}$$

$$\mathbf{u} = \frac{-\kappa(\phi)}{\mu} \nabla p, \quad (x, y) \in \Omega, \quad 0 < t \leq T, \tag{2.2}$$

$$\frac{\partial(\phi c_f)}{\partial t} + \nabla \cdot (\mathbf{u} c_f) = \nabla \cdot (\phi \mathbf{D} \nabla c_f) + k_c a_v (c_s - c_f) + f_I c_I - f_P c_f, \tag{2.3}$$

$$\frac{\partial \phi}{\partial t} = \frac{\alpha k_c a_v (c_f - c_s)}{\rho_s}, \quad (x, y) \in \Omega, \quad 0 < t \leq T, \tag{2.4}$$

where \mathbf{u} and p are the Darcy’s velocity (the volume of flow crossing a unit across-section per unit time) and the pressure in the fluid mixture, respectively. ϕ is the porosity (the percentage of the empty space in a rock) and c_f is the concentrations of acid in the fluid phase. The above variables are unknown time-dependent variables throughout this paper. $f = f_I - f_P$ is the external volumetric flow rate with $f_I = \max\{f, 0\}$ and $f_P = -\min\{f, 0\}$ being the injection flow rate and the production flow rate, respectively. c_I is the concentrations of acid in the injected flow. \mathbf{D} , a positive definite matrix, is the dispersion tensor for the acid in porous media. If the flow vectors are essentially parallel to the x -axis [8,23] or we consider molecular diffusion only [4,32], then \mathbf{D} can be a diagonal matrix. In this paper, we only consider the simplified cases and assume \mathbf{D} to be a diagonal matrix. In this paper, \mathbf{D} , f , f_I , f_P , c_I are given functions. μ is the viscosity of fluid, k_c is the local mass-transfer coefficient and k_s is the kinetic constant for reaction. ρ_s is the density of the rock and α is the dissolving constant of the acid (grams of solid dissolved per mole of acid reacted). These values are positive constants. c_s is the concentrations of acid in the fluid-solid interface. Moreover, in the case of first order kinetic reaction, the concentration c_s has a simple relationship with c_f :

$$c_s = \frac{c_f}{1 + k_s/k_c}. \tag{2.5}$$

The permeability κ and the interfacial area available for reaction a_v are functions of ϕ defined as

$$\frac{\kappa}{\kappa_0} = \frac{\phi}{\phi_0} \left(\frac{\phi(1 - \phi_0)}{\phi_0(1 - \phi)} \right)^2, \quad \frac{a_v}{a_0} = \frac{1 - \phi}{1 - \phi_0}, \tag{2.6}$$

respectively, where κ_0 , a_0 , and ϕ_0 are the initial values for κ , a_v , ϕ . It is easy to see that the pressure is uniquely determined up to a constant, thus we assume $\int_{\Omega} p \, dx dy = 0$. However, this assumption is not essential. If we define $c_2 = 1 - c_f$, then subtracting (2.3) from (2.1) to obtain a ghost equation satisfied by c_2 :

$$\frac{\partial(\phi c_2)}{\partial t} + \nabla \cdot (\mathbf{u} c_2) = \nabla \cdot (\phi \mathbf{D} \nabla c_2) - k_c a_v (c_s - c_f) + f_I (1 - c_I) - f_P c_2. \tag{2.7}$$

Notice that the convection and diffusion terms in (2.7) and (2.3) are almost the same. The main difference between two equations is the source term. From (2.5) and (2.6), we have $-k_c a_v (c_s - c_f) \geq 0$, which will be benefit to the positivity preserving of the source term. Hence, we can apply the same PP technique to (2.7), leading to the fact that $c_f = 1 - c_2 \leq 1$.

In this paper, we consider periodic boundary condition for simplicity. The initial concentration and porosity are given as

$$c_f(x, y, 0) = c_0(x, y), \quad \phi(x, y, 0) = \phi_0(x, y), \quad (x, y) \in \Omega,$$

where $0 < \phi_{\star} \leq \phi_0(x, y) \leq \phi^{\star} < 1$.

3 The Finite Difference Scheme

In this section, we will construct the FD scheme for incompressible wormhole propagation. We adopt the following spatial discretization for the domain $[0, 2\pi] \times [0, 2\pi]$

$$0 = x_{\frac{1}{2}} < x_{\frac{3}{2}} < \dots < x_{N_x - \frac{1}{2}} < x_{N_x + \frac{1}{2}} = 2\pi, \tag{3.1}$$

$$0 = y_{\frac{1}{2}} < y_{\frac{3}{2}} < \dots < y_{N_y - \frac{1}{2}} < y_{N_y + \frac{1}{2}} = 2\pi. \tag{3.2}$$

Moreover, we define

$$I_{i,k} = \left[x_{i-\frac{1}{2}}, x_{i+\frac{1}{2}} \right] \times \left[y_{k-\frac{1}{2}}, y_{k+\frac{1}{2}} \right], \tag{3.3}$$

as the rectangular cells. The grid centers and grid sizes are denoted as

$$x_i = \frac{1}{2} \left(x_{i-\frac{1}{2}} + x_{i+\frac{1}{2}} \right), \quad \Delta x_i = x_{i+\frac{1}{2}} - x_{i-\frac{1}{2}}, \quad i = 1, \dots, N_x, \tag{3.4}$$

$$y_k = \frac{1}{2} \left(y_{k-\frac{1}{2}} + y_{k+\frac{1}{2}} \right), \quad \Delta y_k = y_{k+\frac{1}{2}} - y_{k-\frac{1}{2}}, \quad k = 1, \dots, N_y. \tag{3.5}$$

In this paper, we apply uniform partition and define $\Delta x = \Delta x_i$ and $\Delta y = \Delta y_k$. This assumption is, unfortunately, essential in the reconstruction procedure [25] of the high-order numerical fluxes.

Let $(\cdot)_{i,k}$ denote the numerical approximation at (x_i, y_k) for simplicity. Then the semi-discrete conservative FD scheme for (2.1)–(2.4) has the following form

$$\frac{d}{dt} \phi_{i,k} = -\frac{1}{\Delta x} \left(\hat{u}_{i+\frac{1}{2},k} - \hat{u}_{i-\frac{1}{2},k} \right) - \frac{1}{\Delta y} \left(\hat{v}_{i,k+\frac{1}{2}} - \hat{v}_{i,k-\frac{1}{2}} \right) + f_{i,k}, \tag{3.6}$$

$$a(\phi_{i,k}) u_{i,k} = -\frac{1}{\Delta x} \left(\hat{p}_{i+\frac{1}{2},k} - \hat{p}_{i-\frac{1}{2},k} \right), \tag{3.7}$$

$$a(\phi_{i,k}) v_{i,k} = -\frac{1}{\Delta y} \left(\hat{p}_{i,k+\frac{1}{2}} - \hat{p}_{i,k-\frac{1}{2}} \right), \tag{3.8}$$

$$\begin{aligned} \frac{d}{dt} r_{i,k} = & -\frac{1}{\Delta x} \left(\widehat{C}_{x_{i+\frac{1}{2},k}} - \widehat{C}_{x_{i-\frac{1}{2},k}} \right) - \frac{1}{\Delta y} \left(\widehat{C}_{y_{i,k+\frac{1}{2}}} - \widehat{C}_{y_{i,k-\frac{1}{2}}} \right) \\ & + \frac{1}{\Delta x} \left(\widehat{D}_{x_{i+\frac{1}{2},k}} - \widehat{D}_{x_{i-\frac{1}{2},k}} \right) \\ & + \frac{1}{\Delta y} \left(\widehat{D}_{y_{i,k+\frac{1}{2}}} - \widehat{D}_{y_{i,k-\frac{1}{2}}} \right) - B_1(\phi_{i,k}) c_{f_{i,k}} + f_{I_{i,k}} c_{I_{i,k}} - f_{P_{i,k}} c_{f_{i,k}}, \end{aligned} \tag{3.9}$$

$$\frac{d}{dt} \phi_{i,k} = B_2(\phi_{i,k}) c_{f_{i,k}}, \tag{3.10}$$

where

$$a(\phi) = \frac{\mu}{\kappa(\phi)}, \quad B_1(\phi) = \frac{\alpha_0(1-\phi)k_c k_s}{(1-\phi_0)(k_c + k_s)}, \quad B_2(\phi) = \frac{\alpha \alpha_0(1-\phi)k_c k_s}{\rho_s(1-\phi_0)(k_c + k_s)},$$

with $r = \phi c_f$. Note that since the porosity ϕ is increasing during time evolution and less than 1, $\kappa(\phi)$ is obviously not zero when $0 < \phi_0 < 1$. We denote $(\hat{\cdot})_{i-\frac{1}{2},k}$ as the numerical fluxes at $(x_{i-\frac{1}{2}}, y_k)$ and use it for the spatial derivative along x -axis. Likewise for the other numerical fluxes.

The following definition is essential in constructing suitable numerical fluxes for the BP technique.

Definition 3.1 We say the flux \widehat{C}_x is consistent with \widehat{u} if $\widehat{C}_x = \widehat{u}$ when $c_f = 1$ in Ω .

In [3,13,31], we constructed \widehat{u} and \widehat{v} to be consistent with \widehat{C}_x and \widehat{C}_y in (3.11), respectively, for the DG methods. However, the idea is not straightforward extendable to FD methods, see [11] for detailed explanations.

We first demonstrate the construction of the numerical flux \widehat{C}_x for the convection term. To construct \widehat{C}_x , we select a stencil $I = \{x_{i-r}, \dots, x_{i+1+s}\}$, where $r + s + 1 = m$ is the order of accuracy of the scheme. Generally, we want $r = s$. Then, we apply the flux splitting [25] to the scheme and have

$$\widehat{C}_{x_{i+\frac{1}{2},k}} = \frac{1}{2} \left(\widehat{C}_{x_{i+\frac{1}{2},k}}^+ + \widehat{C}_{x_{i+\frac{1}{2},k}}^- \right), \tag{3.11}$$

where

$$\widehat{C}_{x_{i+\frac{1}{2},k}}^+ = f^+((uc_f)_{i-r,k} + \alpha_C(c_f)_{i-r,k}, \dots, (uc_f)_{i+s,k} + \alpha_C(c_f)_{i+s,k}),$$

and

$$\widehat{C}_{x_{i+\frac{1}{2},k}}^- = f^-((uc_f)_{i+1-r,k} - \alpha_C(c_f)_{i+1-r,k}, \dots, (uc_f)_{i+1+s,k} - \alpha_C(c_f)_{i+1+s,k}),$$

with $\alpha_C = \max_i |u_{i,k}|$. f^\pm , the reconstruction function, has been well-developed in [25] and the reconstruction procedure has been introduced in the Appendix in [11]. Here, we will only demonstrate the following useful property without more details:

$$f^+(a_{-r}, \dots, a_s) = \sum_{\ell=-r}^s \omega_\ell^+ a_\ell, \tag{3.12}$$

$$f^-(a_{1-r}, \dots, a_{1+s}) = \sum_{\ell=1-r}^{s+1} \omega_\ell^- a_\ell, \tag{3.13}$$

where ω_ℓ^\pm is the weights in the reconstruction procedure, which can be obtained by following the algorithm introduced in [25]. The most commonly used reconstruct procedure is based on the weight essential non-oscillatory (WENO) scheme [2,15,20,25,26]. However, with WENO reconstruction procedure, it may not be easy to obtain consistent numerical fluxes. In fact, the nonlinear weights for \widehat{C}_x depend on u , which is obtained from (3.6)–(3.8). Due to the consistency requirement, the nonlinear weights used in the construction of \widehat{u} also depend on u itself. Therefore, we need the values of u to construct the weights for \widehat{u} then solve for u . This contradiction is not easy to fix, and needs further investigations. In this paper, instead of using the nonlinear weights from the WENO algorithm, we adopt the linear weights since those weights are determined by the accuracy of the scheme, not the values of u . The values of the linear weights can be found in Table 2.1 in [25]. It is easy to prove that

$$\sum_{\ell=-r}^s \omega_\ell^+ = \sum_{\ell=1-r}^{s+1} \omega_\ell^- = 1. \tag{3.14}$$

This fact is useful in the construction of consistent numerical flux \widehat{u} and consistent lower-order numerical fluxes in the flux limiters.

The following lemma is essential to construct the consistent numerical flux \widehat{u} and the first-order numerical fluxes for the convection term. Here, we only demonstrate the results, since it has already been proved in [11].

Lemma 3.2 *Let f^\pm be given in (3.12) and (3.13), then we have*

$$f^+(u_{i-r}c_f + \alpha_C c_f, \dots, u_{i+s}c_f + \alpha_C c_f) = f^+(u_{i-r}, \dots, u_{i+s})c_f + \alpha_C c_f,$$

and

$$f^-(u_{i+1-r}c_f - \alpha_C c_f, \dots, u_{i+1+s}c_f - \alpha_C c_f) = f^-(u_{i+1-r}, \dots, u_{i+1+s})c_f - \alpha_C c_f.$$

Now, we proceed to construct the numerical fluxes of Darcy’s velocity \mathbf{u} and pressure p . For the incompressible wormhole propagation, since the initial values of \mathbf{u} and p are not given, we can obtain numerical approximations of these two variables by solving a large system of linear equations at each time level.

Here, unlike [11], we cannot simply take $c_f = 1$ in \widehat{C}_x to obtain the consistent numerical flux \hat{u} . Due to the consistency requirement of the BP technique, we choose \hat{u} as

$$\hat{u}_{i+\frac{1}{2},k} = \frac{1}{2} \left(\hat{u}_{i+\frac{1}{2},k}^+ + \hat{u}_{i+\frac{1}{2},k}^- \right), \tag{3.15}$$

where

$$\hat{u}_{i+\frac{1}{2},k}^+ = f^+(u_{i-r,k}, \dots, u_{i+s,k}), \quad \hat{u}_{i+\frac{1}{2},k}^- = f^-(u_{i+1-r,k}, \dots, u_{i+1+s,k}).$$

Likewise for \hat{v} . By Lemma 3.2, we can easily get that the flux \widehat{C}_x is consistent with \hat{u} .

Next, we will discuss the numerical flux $\hat{p}_{i-\frac{1}{2},k}$. We can simply follow the same construction procedure in computing $\hat{u}_{i-\frac{1}{2},k}$. The flux $\hat{p}_{i,k-\frac{1}{2}}$ can be obtained in similar way.

For the diffusion part, we consider $\widehat{D}_{x_{i+\frac{1}{2},k}} = \widehat{D}_{x_{i+\frac{1}{2},k}}(c_f)$ only, and $\widehat{D}_{y_{i,k+\frac{1}{2}}}$ can be obtained following the same lines with some minor changes. We assume $\mathbf{D} = \text{diag}\{D_{11}, D_{22}\}$ and apply the Taylor’s expansion introduced in [26] to write

$$\begin{aligned} \widehat{D}_{x_{i+\frac{1}{2},k}} &= \phi D_{11} c_{f,x} |_{x_{i+\frac{1}{2}},y_k} - \frac{\Delta x^2}{24} \frac{\partial^2}{\partial x^2} (\phi D_{11} c_{f,x}) |_{x_{i+\frac{1}{2}},y_k} \\ &\quad + \frac{7\Delta x^4}{5760} \frac{\partial^4}{\partial x^4} (\phi D_{11} c_{f,x}) |_{x_{i+\frac{1}{2}},y_k}. \end{aligned} \tag{3.16}$$

To evaluate \widehat{D}_x , we use the point values of ϕ , c_f and u within the stencil I to construct the polynomials interpolation of ϕ , D_{11} and c_f , denoted as p_ϕ , p_{11} and p_c , respectively. Then $p^x = p_\phi p_{11} (p_c)_x$ is a high-order approximation of $\phi D_{11} c_{f,x}$. The approximations of $\phi D_{11} c_{f,x}$ and its derivatives can be obtained by reading the point values of p^x as well as its derivatives. For example, in order to consistent with the fifth order scheme ($m = 5$), we want p_c to be a sixth order approximation of c_f , and then we should use a stencil with six points.

Remark 3.3 The sequence of solving (3.6)–(3.10) can be summarized as follows:

1. We directly use ϕ^n , c_f^n and (3.10) to obtain ϕ_t^n , which further yield ϕ^{n+1} .
2. Then we take the ϕ_t^n solved in step 1 as the source term in equation (3.6). Therefore, we can combine Eqs. (3.6)–(3.8) to form a large system of linear equations for p . By solving this large system of linear equations at time level n , we can obtain p^n and \mathbf{u}^n .
3. Finally, we construct the numerical fluxes in (3.9) with ϕ^n , c_f^n and \mathbf{u}^n . Thus, we can get r_t^n . Moreover, we can obtain c_f^{n+1} with $r = \phi c_f$.

Remark 3.4 Thanks to the consistent numerical fluxes, we can subtract (3.9) from (3.6) to obtain the numerical scheme satisfied by $c_2 = 1 - c_f$ (or $r_2 = \phi - r$):

$$\begin{aligned} \frac{d}{dt} r_{2i,k} = & -\frac{1}{\Delta x} (\widehat{C}_{x_{2i+\frac{1}{2},k}} - \widehat{C}_{x_{2i-\frac{1}{2},k}}) - \frac{1}{\Delta y} (\widehat{C}_{y_{2i,k+\frac{1}{2}}} - \widehat{C}_{y_{2i,k-\frac{1}{2}}}) \\ & + \frac{1}{\Delta x} (\widehat{D}_{x_{2i+\frac{1}{2},k}} - \widehat{D}_{x_{2i-\frac{1}{2},k}}) \\ & + \frac{1}{\Delta y} (\widehat{D}_{y_{2i,k+\frac{1}{2}}} - \widehat{D}_{y_{2i,k-\frac{1}{2}}}) + B_1(\phi_{i,k})c_{f_{i,k}} + f_{I_{i,k}}(1 - c_{I_{i,k}}) - f_{P_{i,k}}c_{2i,k}. \end{aligned} \tag{3.17}$$

where $\widehat{D}_{x_2}(c_2) = -\widehat{D}_x(c_f)$, $\widehat{D}_{y_2}(c_2) = -\widehat{D}_y(c_f)$. We can apply the PP technique to (3.17) to obtain positive c_2 (or r_2), leading to $c_f \leq 1$.

Remark 3.5 Due to the consistency requirement, \hat{u} is taken as the central flux without penalty, likewise for \hat{v} and \hat{p} . However, in numerical simulations, we cannot use even number of grid points for the partition of the computational domain. We use the following linear heat equation in one dimension as an example to demonstrate the reason:

$$u_x = 0, \quad u = p_x, \quad x \in \Omega,$$

subject to periodic boundary condition and $\int_{\Omega} p dx = 0$. With central flux, the second-order spatial discretization is given as

$$u_{j+1} - u_{j-1} = 0, \quad u_j = p_{j+1} - p_{j-1},$$

then we can obtain

$$p_{j+2} - 2p_j + p_{j-2} = 0.$$

Even with the additional condition that $\sum_j p_j = 0$, the above is not uniquely solvable if even number of grid points is used. To handle this difficulty, we choose odd number of points in both x and y directions in all the numerical simulations.

Finally, we want to demonstrate the following key ideas.

1. Since ϕ must be between 0 and 1 and increase monotonically, we will first apply positivity-preserving technique to obtain positive ϕ_l and use which as another source to find the velocity and pressure.
2. Due to the initial values of \mathbf{u} and p are not given, we need to couple the equations satisfied by \mathbf{u} and p to obtain the numerical approximations of these two variables. Then, we construct special numerical fluxes \hat{u} and \hat{v} which are consistent with \widehat{C}_x and \widehat{C}_y , respectively.
3. Apply flux limiters to the high-order scheme by taking a linear combination of the first-order and high-order fluxes. These two numerical fluxes use the same stencils.
4. For diffusion part, apply Taylor’s expansion to construct the numerical fluxes.

4 Bound-Preserving Technique

In this section, we proceed to discuss the BP technique for problems in two space dimensions. Though the FD scheme can provide high-order approximation, it may not preserve the physical bounds of the numerical solution. In order to construct the BP technique, we

consider the semi-discrete conservative FD scheme (3.6)–(3.10). We apply a parameterized PP flux limiter to modify the high-order fluxes in (3.9) towards a first-order fluxes by taking a linear combination of them. We would like to prove that the first-order scheme maintains the positivity of the numerical approximations with the appropriate time steps. Following the analysis in [3,13], the numerical solution c_f can be bounded between 0 and 1 by using the consistent numerical flux pair.

4.1 First-Order Scheme

In this subsection, we will construct first-order BP technique with Euler forward time discretization. The first-order form of (3.9) can be written as

$$\begin{aligned} \frac{d}{dt}r_{i,k} &= -\frac{1}{\Delta x} \left(\widehat{c}_{x_{i+\frac{1}{2},k}} - \widehat{c}_{x_{i-\frac{1}{2},k}} \right) - \frac{1}{\Delta y} \left(\widehat{c}_{y_{i,k+\frac{1}{2}}} - \widehat{c}_{y_{i,k-\frac{1}{2}}} \right) \\ &\quad + \frac{1}{\Delta x} \left(\widehat{d}_{x_{i+\frac{1}{2},k}} - \widehat{d}_{x_{i-\frac{1}{2},k}} \right) + \frac{1}{\Delta y} \left(\widehat{d}_{y_{i,k+\frac{1}{2}}} - \widehat{d}_{y_{i,k-\frac{1}{2}}} \right) \\ &\quad - B_1(\phi_{i,k})c_{f_{i,k}} + f_{I_{i,k}}c_{I_{i,k}} - f_{P_{i,k}}c_{f_{i,k}}, \end{aligned} \tag{4.1}$$

where \widehat{c}_x , \widehat{c}_y , \widehat{d}_x and \widehat{d}_y are the first-order numerical fluxes. We define o^n to represent the numerical approximation of o at time level n . In the rest of this section, for the numerical approximations at time level n , we will drop the superscript n for simplicity. Then the first-order fully-discretized scheme of (4.1) has the following form

$$r_{i,k}^{n+1} = F_{i,k}^c + F_{i,k}^d + F_{i,k}^s, \tag{4.2}$$

where

$$F_{i,k}^c = \frac{1}{3}r_{i,k} - \lambda_x \left(\widehat{c}_{x_{i+\frac{1}{2},k}} - \widehat{c}_{x_{i-\frac{1}{2},k}} \right) - \lambda_y \left(\widehat{c}_{y_{i,k+\frac{1}{2}}} - \widehat{c}_{y_{i,k-\frac{1}{2}}} \right), \tag{4.3}$$

$$F_{i,k}^d = \frac{1}{3}r_{i,k} + \lambda_x \left(\widehat{d}_{x_{i+\frac{1}{2},k}} - \widehat{d}_{x_{i-\frac{1}{2},k}} \right) + \lambda_y \left(\widehat{d}_{y_{i,k+\frac{1}{2}}} - \widehat{d}_{y_{i,k-\frac{1}{2}}} \right), \tag{4.4}$$

$$F_{i,k}^s = \frac{1}{3}r_{i,k} + \Delta t \left(f_{I_{i,k}}c_{I_{i,k}} - B_1(\phi_{i,k})c_{f_{i,k}} - f_{P_{i,k}}c_{f_{i,k}} \right), \tag{4.5}$$

with $\lambda_x = \frac{\Delta t}{\Delta x}$ and $\lambda_y = \frac{\Delta t}{\Delta y}$ being the ratio of the time and space mesh sizes along x and y directions, respectively.

Now, we proceed to construct the first-order numerical fluxes. For convection part, we need to take the special low-order numerical fluxes $\widehat{c}_{x_{i+\frac{1}{2},k}}$ and $\widehat{c}_{y_{i,k+\frac{1}{2}}}$ such that $\widehat{c}_x = \widehat{u}$ and $\widehat{c}_y = \widehat{v}$ when $c_f = 1$, respectively. Following the construction in (3.11), we take

$$\widehat{c}_{x_{i+\frac{1}{2},k}} = \frac{1}{2} \left(\left(\widehat{f}_{i+\frac{1}{2},k}^+ + \alpha_x \right) c_{f_{i,k}} + \left(\widehat{f}_{i+\frac{1}{2},k}^- - \alpha_x \right) c_{f_{i+1,k}} \right), \tag{4.6}$$

$$\widehat{c}_{y_{i,k+\frac{1}{2}}} = \frac{1}{2} \left(\left(\widehat{f}_{i,k+\frac{1}{2}}^+ + \alpha_y \right) c_{f_{i,k}} + \left(\widehat{f}_{i,k+\frac{1}{2}}^- - \alpha_y \right) c_{f_{i,k+1}} \right), \tag{4.7}$$

where

$$\widehat{f}_{i+\frac{1}{2},k}^+ = f^+(u_{i-r,k}, \dots, u_{i+s,k}), \quad \widehat{f}_{i+\frac{1}{2},k}^- = f^-(u_{i-r+1,k}, \dots, u_{i+s+1,k}).$$

$\hat{f}_{i,k+\frac{1}{2}}^+$ and $\hat{f}_{i,k+\frac{1}{2}}^-$ can be defined analogously. The parameters α_x and α_y being determined by the BP technique. By Lemma 3.2, it is easy to verify that $\hat{c}_{x_{i+\frac{1}{2},k}}$ and $\hat{c}_{y_{i,k+\frac{1}{2}}}$ are consistent with \hat{u} and \hat{v} , respectively.

For diffusion term, the numerical fluxes can be taken as

$$\hat{d}_{x_{i+\frac{1}{2},k}} = \left(\bar{D}_{i+\frac{1}{2},k}^{11} \right) \frac{c_{f_{i+1,k}} - c_{f_{i,k}}}{\Delta x}, \quad \hat{d}_{y_{i,k+\frac{1}{2}}} = \left(\bar{D}_{i,k+\frac{1}{2}}^{22} \right) \frac{c_{f_{i,k+1}} - c_{f_{i,k}}}{\Delta y},$$

where $\bar{D}_{i+\frac{1}{2},k}^{11} = \frac{1}{2} ((\phi D_{11}(\mathbf{u}))_{i,k} + (\phi D_{11}(\mathbf{u}))_{i+1,k})$. Likewise for $\bar{D}_{i,k+\frac{1}{2}}^{22}$.

Next, we proceed to prove that the first-order scheme is bound-preserving. Firstly, we demonstrate some properties for porosity ϕ in the following theorem:

Theorem 4.1 *Given $0 \leq r_{i,k} \leq \phi_{i,k}$ ($0 \leq c_{f_{i,k}} \leq 1$) and $\phi_{i,k} < 1$ for all i, k , we have $\phi_{i,k} \leq \phi_{i,k}^{n+1} < 1$, if the time step satisfies*

$$\Delta t < B^{-1}, \tag{4.8}$$

where B is a positive constant defined as

$$B = \frac{\alpha a_0 k_c k_s}{\rho_s (1 - \phi^*) (k_c + k_s)}.$$

Proof We define $B_3(x, y) = \frac{\alpha a_0 k_c k_s}{\rho_s (1 - \phi_0(x, y)) (k_c + k_s)}$, which is independent of time t and is greater than 0. Thus, we have $B_2(\phi) = B_3(x, y) \cdot (1 - \phi) \leq B \cdot (1 - \phi)$.

It is easy to prove that

$$\begin{aligned} \phi_{i,k}^{n+1} &= \phi_{i,k} + \Delta t B_2(\phi_{i,k}) c_{f_{i,k}} \\ &= \phi_{i,k} + \Delta t B_3(x, y) \cdot (1 - \phi_{i,k}) c_{f_{i,k}} \\ &\geq \phi_{i,k}, \end{aligned}$$

where we use the assumption $\phi_{i,k} < 1$ and $0 \leq c_{f_{i,k}} \leq 1$. Moreover, we have

$$\begin{aligned} \phi_{i,k}^{n+1} &= \phi_{i,k} + \Delta t B_2(\phi_{i,k}) c_{f_{i,k}} \\ &= \phi_{i,k} + \Delta t B_3(x, y) \cdot (1 - \phi_{i,k}) c_{f_{i,k}} \\ &\leq \phi_{i,k} + \Delta t B \cdot (1 - \phi_{i,k}) \\ &= (1 - \Delta t B) \phi_{i,k} + \Delta t B. \end{aligned}$$

Clearly, under the condition (4.8), we can obtain $\phi_{i,k}^{n+1} < 1$. □

Since ϕc_f on the left hand side in (3.9) has been replaced by a new variable r , we discuss the bound-preserving property of r instead of c_f . In the following lemmas, we will study the PP property of r in (4.2). We analyze $F_{i,k}^c$ first.

Lemma 4.2 *Assume $c_{f_{i,k}} > 0$ for all i and k , then $F_{i,k}^c > 0$ under the conditions*

$$\lambda_x = \frac{\Delta t}{\Delta x} \leq \frac{\phi_{i,k}}{3 \left(\hat{f}_{i+\frac{1}{2},k}^+ - \hat{f}_{i-\frac{1}{2},k}^- + 2\alpha_x \right)}, \quad \lambda_y = \frac{\Delta t}{\Delta y} \leq \frac{\phi_{i,k}}{3 \left(\hat{f}_{i,k+\frac{1}{2}}^+ - \hat{f}_{i,k-\frac{1}{2}}^- + 2\alpha_y \right)}, \tag{4.9}$$

and

$$\alpha_x \geq \max_{i,k} \left\{ -\hat{f}_{i+\frac{1}{2},k}^+, \hat{f}_{i+\frac{1}{2},k}^-, 0 \right\}, \quad \alpha_y \geq \max_{i,k} \left\{ -\hat{f}_{i,k+\frac{1}{2}}^+, \hat{f}_{i,k+\frac{1}{2}}^-, 0 \right\}. \tag{4.10}$$

Proof It is easy to prove that

$$\begin{aligned} F_{i,k}^c &= \frac{1}{3}r_{i,k} - \lambda_x \left(\hat{c}_{x_{i+\frac{1}{2},k}} - \hat{c}_{x_{i-\frac{1}{2},k}} \right) - \lambda_y \left(\hat{c}_{y_{i,k+\frac{1}{2}}} - \hat{c}_{y_{i,k-\frac{1}{2}}} \right) \\ &= \frac{1}{6}r_{i,k} - \lambda_x \left(\hat{c}_{x_{i+\frac{1}{2},k}} - \hat{c}_{x_{i-\frac{1}{2},k}} \right) + \frac{1}{6}r_{i,k} - \lambda_y \left(\hat{c}_{y_{i,k+\frac{1}{2}}} - \hat{c}_{y_{i,k-\frac{1}{2}}} \right) \\ &= L_x^c + L_y^c, \end{aligned}$$

where

$$\begin{aligned} L_x^c &= \frac{1}{6}\phi_{i,k}c_{f_{i,k}} \\ &\quad - \frac{\lambda_x}{2} \left(\left(\hat{f}_{i+\frac{1}{2},k}^+ + \alpha_x \right) c_{f_{i,k}} + \left(\hat{f}_{i+\frac{1}{2},k}^- - \alpha_x \right) c_{f_{i+1,k}} \right. \\ &\quad \left. - \left(\hat{f}_{i-\frac{1}{2},k}^+ + \alpha_x \right) c_{f_{i-1,k}} - \left(\hat{f}_{i-\frac{1}{2},k}^- - \alpha_x \right) c_{f_{i,k}} \right) \\ &= \left(\frac{1}{6}\phi_{i,k} - \frac{\lambda_x}{2} \left(\hat{f}_{i+\frac{1}{2},k}^+ - \hat{f}_{i-\frac{1}{2},k}^- + 2\alpha_x \right) \right) c_{f_{i,k}} \\ &\quad + \frac{\lambda_x}{2} \left(\alpha_x - \hat{f}_{i+\frac{1}{2},k}^- \right) c_{f_{i+1,k}} + \frac{\lambda_x}{2} \left(\alpha_x + \hat{f}_{i-\frac{1}{2},k}^+ \right) c_{f_{i-1,k}}, \end{aligned}$$

and

$$\begin{aligned} L_y^c &= \frac{1}{6}\phi_{i,k}c_{f_{i,k}} \\ &\quad - \frac{\lambda_y}{2} \left(\left(\hat{f}_{i,k+\frac{1}{2}}^+ + \alpha_y \right) c_{f_{i,k}} + \left(\hat{f}_{i,k+\frac{1}{2}}^- - \alpha_y \right) c_{f_{i,k+1}} - \left(\hat{f}_{i,k-\frac{1}{2}}^+ + \alpha_y \right) c_{f_{i,k-1}} \right. \\ &\quad \left. - \left(\hat{f}_{i,k-\frac{1}{2}}^- - \alpha_y \right) c_{f_{i,k}} \right) \\ &= \left(\frac{1}{6}\phi_{i,k} - \frac{\lambda_y}{2} \left(\hat{f}_{i,k+\frac{1}{2}}^+ - \hat{f}_{i,k-\frac{1}{2}}^- + 2\alpha_y \right) \right) c_{f_{i,k}} \\ &\quad + \frac{\lambda_y}{2} \left(\alpha_y - \hat{f}_{i,k+\frac{1}{2}}^- \right) c_{f_{i,k+1}} + \frac{\lambda_y}{2} \left(\alpha_y + \hat{f}_{i,k-\frac{1}{2}}^+ \right) c_{f_{i,k-1}}. \end{aligned}$$

Thus, under the conditions (4.9) and (4.10), all the coefficients are positive. Hence, we have $L_x^c > 0$ and $L_y^c > 0$, which further yields $F_{i,k}^c > 0$. □

Now, we proceed to prove $F_{i,k}^d > 0$.

Lemma 4.3 Assume $c_{f_{i,k}} > 0$ for all i and k , then $F_{i,k}^d > 0$ under the conditions

$$\Lambda_x = \frac{\Delta t}{\Delta x^2} \leq \frac{\phi_{i,k}}{12D_{11}^M}, \quad \Lambda_y = \frac{\Delta t}{\Delta y^2} \leq \frac{\phi_{i,k}}{12D_{22}^M}, \tag{4.11}$$

where

$$D_{\ell\ell}^M = \max_{i,k} ((\phi D_{\ell\ell}(\mathbf{u}))_{i,k}), \quad \ell = 1, 2.$$

Proof Based on the same analysis of the convection term, we have

$$\begin{aligned}
 F_{i,k}^d &= \frac{1}{3}r_{i,k} + \lambda_x(\widehat{d}_{x_{i+\frac{1}{2},k}} - \widehat{d}_{x_{i-\frac{1}{2},k}}) + \lambda_y(\widehat{d}_{y_{i,k+\frac{1}{2}}} - \widehat{d}_{y_{i,k-\frac{1}{2}}}) \\
 &= \frac{1}{3}\phi_{i,k}c_{f_{i,k}} + \lambda_x(\widehat{d}_{x_{i+\frac{1}{2},k}} - \widehat{d}_{x_{i-\frac{1}{2},k}}) + \lambda_y(\widehat{d}_{y_{i,k+\frac{1}{2}}} - \widehat{d}_{y_{i,k-\frac{1}{2}}}) = L_x^d + L_y^d,
 \end{aligned}$$

where

$$\begin{aligned}
 L_x^d &= \frac{1}{6}\phi_{i,k}c_{f_{i,k}} + \lambda_x(\widehat{d}_{x_{i+\frac{1}{2},k}} - \widehat{d}_{x_{i-\frac{1}{2},k}}) \\
 &= \frac{1}{6}\phi_{i,k}c_{f_{i,k}} + \frac{\Delta t}{\Delta x} \left(\frac{(\phi D_{11}(\mathbf{u}))_{i,k} + (\phi D_{11}(\mathbf{u}))_{i+1,k}}{2} \frac{c_{f_{i+1,k}} - c_{f_{i,k}}}{\Delta x} \right) \\
 &\quad - \frac{\Delta t}{\Delta x} \left(\frac{(\phi D_{11}(\mathbf{u}))_{i-1,k} + (\phi D_{11}(\mathbf{u}))_{i,k}}{2} \frac{c_{f_{i,k}} - c_{f_{i-1,k}}}{\Delta x} \right) \\
 &= \left(\frac{1}{6}\phi_{i,k} - \frac{\Lambda_x}{2} ((\phi D_{11}(\mathbf{u}))_{i-1,k} + 2(\phi D_{11}(\mathbf{u}))_{i,k} + (\phi D_{11}(\mathbf{u}))_{i+1,k}) \right) c_{f_{i,k}} \\
 &\quad + \frac{\Lambda_x}{2} ((\phi D_{11}(\mathbf{u}))_{i,k} + (\phi D_{11}(\mathbf{u}))_{i+1,k}) c_{f_{i+1,k}} \\
 &\quad + \frac{\Lambda_x}{2} ((\phi D_{11}(\mathbf{u}))_{i-1,k} + (\phi D_{11}(\mathbf{u}))_{i,k}) c_{f_{i-1,k}},
 \end{aligned}$$

and

$$\begin{aligned}
 L_y^d &= \frac{1}{6}\phi_{i,k}c_{f_{i,k}} + \lambda_y(\widehat{d}_{y_{i,k+\frac{1}{2}}} - \widehat{d}_{y_{i,k-\frac{1}{2}}}) \\
 &= \frac{1}{6}\phi_{i,k}c_{f_{i,k}} + \frac{\Delta t}{\Delta y} \left(\frac{(\phi D_{22}(\mathbf{u}))_{i,k} + (\phi D_{22}(\mathbf{u}))_{i,k+1}}{2} \frac{c_{f_{i,k+1}} - c_{f_{i,k}}}{\Delta y} \right) \\
 &\quad - \frac{\Delta t}{\Delta y} \left(\frac{(\phi D_{22}(\mathbf{u}))_{i,k-1} + (\phi D_{22}(\mathbf{u}))_{i,k}}{2} \frac{c_{f_{i,k}} - c_{f_{i,k-1}}}{\Delta y} \right) \\
 &= \left(\frac{1}{6}\phi_{i,k} - \frac{\Lambda_y}{2} ((\phi D_{22}(\mathbf{u}))_{i,k-1} + 2(\phi D_{22}(\mathbf{u}))_{i,k} + (\phi D_{22}(\mathbf{u}))_{i,k+1}) \right) c_{f_{i,k}} \\
 &\quad + \frac{\Lambda_y}{2} ((\phi D_{22}(\mathbf{u}))_{i,k} + (\phi D_{22}(\mathbf{u}))_{i,k+1}) c_{f_{i,k+1}} \\
 &\quad + \frac{\Lambda_y}{2} ((\phi D_{22}(\mathbf{u}))_{i,k-1} + (\phi D_{22}(\mathbf{u}))_{i,k}) c_{f_{i,k-1}}.
 \end{aligned}$$

Since $(\phi D(\mathbf{u}))_{i,k} \geq 0$ for all i and k , we have $L_x^d > 0$ and $L_y^d > 0$ under the condition (4.11). Thus, we can obtain $F_{i,k}^d > 0$. □

Next, we will prove $F_{i,k}^s > 0$.

Lemma 4.4 Assume $c_{f_{i,k}} > 0$ for all i and k , then $F_{i,k}^s > 0$ if the time step satisfies

$$\Delta t \leq \min\left\{ \frac{\phi_\star}{6B_1(\phi_\star)}, \frac{\phi_\star}{6f_{PM}} \right\}, \tag{4.12}$$

where

$$f_{PM} = \max_{i,k} f_{P_{i,k}}. \tag{4.13}$$

Proof The source term can be split into

$$F_{i,k}^s = \frac{1}{3}r_{i,k} + \Delta t(f_{I_{i,k}}c_{I_{i,k}} - B_1(\phi_{i,k})c_{f_{i,k}} - f_{P_{i,k}}c_{f_{i,k}})$$

$$\begin{aligned}
 &= \Delta t f_{I_{i,k}} c_{I_{i,k}} + \frac{1}{6} r_{i,k} - \Delta t B_1(\phi_{i,k}) c_{f_{i,k}} + \frac{1}{6} r_{i,k} - \Delta t f_{P_{i,k}} c_{f_{i,k}} \\
 &= \Delta t f_{I_{i,k}} c_{I_{i,k}} + \left(\frac{1}{6} \phi_{i,k} - \Delta t B_1(\phi_{i,k}) \right) c_{f_{i,k}} + \left(\frac{1}{6} \phi_{i,k} - \Delta t f_{P_{i,k}} \right) c_{f_{i,k}} \\
 &= S^1 + S^2 + S^3.
 \end{aligned}$$

Clearly, it is easy to verify that $S^1 = \Delta t f_{I_{i,k}} c_{I_{i,k}} \geq 0$. Then under the condition (4.12), We have $S^2 > 0$ and $S^3 > 0$. To sum up, $F_{i,k}^s = S^1 + S^2 + S^3 > 0$ under the condition (4.12). \square

Combining the above three lemmas, we can obtain the following theorem.

Theorem 4.5 Consider the FD scheme (3.6)–(3.8), (4.1) and (3.10) with Euler forward time discretization. Assume $c_{f_{i,k}} > 0$ for all i and k , then $r_{i,k}^{n+1} > 0$, $L_x^c + L_x^d + \frac{1}{2} F_{i,k}^s > 0$ and $L_y^c + L_y^d + \frac{1}{2} F_{i,k}^s > 0$ under the conditions (4.9), (4.10), (4.11) and (4.12).

Proof To obtain $r_{i,k}^{n+1} > 0$, we only need $F_{i,k}^c$, $F_{i,k}^d$, and $F_{i,k}^s$ in (4.2) to be positive, which follows directly from Lemmas 4.2–4.4, respectively. Meanwhile, $L_x^c + L_x^d + \frac{1}{2} F_{i,k}^s > 0$ and $L_y^c + L_y^d + \frac{1}{2} F_{i,k}^s > 0$ used in BP technique can be derived from Lemmas 4.2–4.4. \square

From Theorem 4.5, we have $r^{n+1} > 0$ over the computational domain. Moreover, we also need to prove $r^{n+1} < \phi^{n+1}$, and the result is as follows.

Theorem 4.6 Suppose all the conditions in Theorem 4.5 are satisfied. We assume $c_{f_{i,k}} > 0$ and $c_{2i,k} > 0$ for all i, k and choose the consistent flux pair (\hat{u}, \hat{c}_x) and (\hat{v}, \hat{c}_y) . Then $0 \leq r^{n+1} \leq \phi^{n+1}$.

Proof Because of the fluxes \hat{u} and \hat{c}_x as well as \hat{v} and \hat{c}_y are consistent, then we can deduce a ghost equation for r_2 by subtracting (4.1) from (3.6) and introducing ghost variables $r_2 = \phi c_2$, $c_2 = 1 - c_f$ and $c_{2I} = 1 - c_I$,

$$\begin{aligned}
 \frac{d}{dt} r_{2i,k} &= -\frac{1}{\Delta x} \left(\widehat{c}_{x_{2i+\frac{1}{2},k}} - \widehat{c}_{x_{2i-\frac{1}{2},k}} \right) - \frac{1}{\Delta y} \left(\widehat{c}_{y_{2i,k+\frac{1}{2}}} - \widehat{c}_{y_{2i,k-\frac{1}{2}}} \right) \\
 &\quad + \frac{1}{\Delta x} \left(\widehat{d}_{x_{2i+\frac{1}{2},k}} - \widehat{d}_{x_{2i-\frac{1}{2},k}} \right) \\
 &\quad + \frac{1}{\Delta y} \left(\widehat{d}_{y_{2i,k+\frac{1}{2}}} - \widehat{d}_{y_{2i,k-\frac{1}{2}}} \right) + B_1(\phi_{i,k}) c_{f_{i,k}} + f_{I_{i,k}} c_{2I_{i,k}} - f_{P_{i,k}} c_{2i,k},
 \end{aligned} \tag{4.14}$$

where \widehat{c}_{x_2} and \widehat{c}_{y_2} are numerical fluxes for the convection part, \widehat{d}_{x_2} and \widehat{d}_{y_2} are numerical fluxes for the diffusion part. Compare the Eq. (4.14) with (3.9), we can find that the equation for r_2 is very similar to that for r . The main difference between two equations is that source term in (4.14) contains a positive term $+B_1(\phi)c_f$ instead of $-B_1(\phi)c_f$, which will relax the restrictions on time steps for PP of the source term. Therefore, following the same analysis in Theorem 4.5, with Euler forward time discretization we can get $r_2^{n+1} > 0$ under the conditions (4.9), (4.10), (4.11) and (4.12), which further yields $r^{n+1} < \phi^{n+1}$. \square

4.2 Bound-Preserving Technique for High-Order Schemes

In this subsection, we will construct high-order BP technique by taking a linear combination of first-order and high-order numerical fluxes with the parameterized PP flux limiter. Here, we also apply Euler forward time discretization.

We write (3.9) as

$$r_{i,k}^{n+1} = r_{i,k} - \lambda_x(\hat{F}_{i+\frac{1}{2},k}^x - \hat{F}_{i-\frac{1}{2},k}^x) - \lambda_y(\hat{F}_{i,k+\frac{1}{2}}^y - \hat{F}_{i,k-\frac{1}{2}}^y) + \Delta t S_{i,k}, \tag{4.15}$$

where

$$\hat{F}_{i+\frac{1}{2},k}^x = \widehat{C}_{x_{i+\frac{1}{2},k}} - \widehat{D}_{x_{i+\frac{1}{2},k}}, \quad \hat{F}_{i,k+\frac{1}{2}}^y = \widehat{C}_{y_{i,k+\frac{1}{2}}} - \widehat{D}_{y_{i,k+\frac{1}{2}}},$$

and

$$S_{i,k} = f_{I_{i,k}cI_{i,k}} - B_1(\phi_{i,k})c_{f_{i,k}} - f_{P_{i,k}cF_{i,k}}.$$

To obtain positive numerical approximation $r_{i,k}^{n+1}$, we replace the numerical fluxes $\hat{F}_{i+\frac{1}{2},k}^x$ and $\hat{F}_{i,k+\frac{1}{2}}^y$ in (4.15) by the modified fluxes

$$\begin{aligned} \tilde{F}_{i+\frac{1}{2},k}^x &= \theta_{i+\frac{1}{2},k} \left(\hat{F}_{i+\frac{1}{2},k}^x - \hat{f}_{i+\frac{1}{2},k}^x \right) + \hat{f}_{i+\frac{1}{2},k}^x, & \tilde{F}_{i,k+\frac{1}{2}}^y &= \theta_{i,k+\frac{1}{2}} \left(\hat{F}_{i,k+\frac{1}{2}}^y - \hat{f}_{i,k+\frac{1}{2}}^y \right) \\ &+ \hat{f}_{i,k+\frac{1}{2}}^y, \end{aligned} \tag{4.16}$$

respectively. In (4.16), $\hat{f}_{i+\frac{1}{2},k}^x = \widehat{c}_{x_{i+\frac{1}{2},k}} - \widehat{d}_{x_{i+\frac{1}{2},k}}$ and $\hat{f}_{i,k+\frac{1}{2}}^y = \widehat{c}_{y_{i,k+\frac{1}{2}}} - \widehat{d}_{y_{i,k+\frac{1}{2}}}$ are the first-order fluxes discussed in Sect. 4.1. We want to choose the limiting parameters $\theta_{i+\frac{1}{2},k} \in [0, 1]$ and $\theta_{i,k+\frac{1}{2}} \in [0, 1]$ such that

$$r_{i,k} - \lambda_x(\tilde{F}_{i+\frac{1}{2},k}^x - \tilde{F}_{i-\frac{1}{2},k}^x) - \lambda_y(\tilde{F}_{i,k+\frac{1}{2}}^y - \tilde{F}_{i,k-\frac{1}{2}}^y) + \Delta t S_{i,k} \geq 0,$$

which can be divided into two parts along the x and y directions, respectively.

$$\frac{1}{2}r_{i,k} - \lambda_x \left(\tilde{F}_{i+\frac{1}{2},k}^x - \tilde{F}_{i-\frac{1}{2},k}^x \right) + \frac{1}{2}\Delta t S_{i,k} \geq 0, \tag{4.17}$$

$$\frac{1}{2}r_{i,k} - \lambda_y \left(\tilde{F}_{i,k+\frac{1}{2}}^y - \tilde{F}_{i,k-\frac{1}{2}}^y \right) + \frac{1}{2}\Delta t S_{i,k} \geq 0. \tag{4.18}$$

We can rewrite these two inequalities as

$$\lambda_x \theta_{i-\frac{1}{2},k} \left(\hat{F}_{i-\frac{1}{2},k}^x - \hat{f}_{i-\frac{1}{2},k}^x \right) - \lambda_x \theta_{i+\frac{1}{2},k} \left(\hat{F}_{i+\frac{1}{2},k}^x - \hat{f}_{i+\frac{1}{2},k}^x \right) - \Gamma_{i,k}^{m_x} \geq 0, \tag{4.19}$$

$$\lambda_y \theta_{i,k-\frac{1}{2}} \left(\hat{F}_{i,k-\frac{1}{2}}^y - \hat{f}_{i,k-\frac{1}{2}}^y \right) - \lambda_y \theta_{i,k+\frac{1}{2}} \left(\hat{F}_{i,k+\frac{1}{2}}^y - \hat{f}_{i,k+\frac{1}{2}}^y \right) - \Gamma_{i,k}^{m_y} \geq 0, \tag{4.20}$$

where

$$\Gamma_{i,k}^{m_x} = -\frac{1}{2}r_{i,k} + \lambda_x \left(\hat{f}_{i+\frac{1}{2},k}^x - \hat{f}_{i-\frac{1}{2},k}^x \right) - \frac{1}{2}\Delta t (f_{I_{i,k}cI_{i,k}} - B_1(\phi_{i,k})c_{f_{i,k}} - f_{P_{i,k}cF_{i,k}}) \leq 0, \tag{4.21}$$

$$\Gamma_{i,k}^{m_y} = -\frac{1}{2}r_{i,k} + \lambda_y \left(\hat{f}_{i,k+\frac{1}{2}}^y - \hat{f}_{i,k-\frac{1}{2}}^y \right) - \frac{1}{2}\Delta t (f_{I_{i,k}cI_{i,k}} - B_1(\phi_{i,k})c_{f_{i,k}} - f_{P_{i,k}cF_{i,k}}) \leq 0. \tag{4.22}$$

Theorem 4.5 guarantees that both $\Gamma_{i,k}^{m_x} \leq 0$ and $\Gamma_{i,k}^{m_y} \leq 0$. For brevity, we define $F_{i\pm\frac{1}{2},k}^x = \hat{F}_{i\pm\frac{1}{2},k}^x - \hat{f}_{i\pm\frac{1}{2},k}^x$ and $F_{i,k\pm\frac{1}{2}}^y = \hat{F}_{i,k\pm\frac{1}{2}}^y - \hat{f}_{i,k\pm\frac{1}{2}}^y$. We consider the node (i, k) and look for the

locally defined pairs of numbers $\left(\Lambda_{-\frac{1}{2}, I_i, k}^m, \Lambda_{+\frac{1}{2}, I_i, k}^m\right)$ along the x direction such that (4.19) is satisfied for

$$\theta_{i-\frac{1}{2}, k} \in \left[0, \Lambda_{-\frac{1}{2}, I_i, k}^m\right], \quad \theta_{i+\frac{1}{2}, k} \in \left[0, \Lambda_{+\frac{1}{2}, I_i, k}^m\right]. \tag{4.23}$$

Following [30],

1. If $F_{i-\frac{1}{2}, k} \geq 0$ and $F_{i+\frac{1}{2}, k} \leq 0$, let

$$\left(\Lambda_{-\frac{1}{2}, I_i, k}^m, \Lambda_{+\frac{1}{2}, I_i, k}^m\right) = (1, 1).$$

2. If $F_{i-\frac{1}{2}, k} \geq 0$ and $F_{i+\frac{1}{2}, k} > 0$, let

$$\left(\Lambda_{-\frac{1}{2}, I_i, k}^m, \Lambda_{+\frac{1}{2}, I_i, k}^m\right) = \left(1, \min\left(1, \frac{\Gamma_{i, k}^{m_x}}{-\lambda F_{i+\frac{1}{2}, k} - \epsilon}\right)\right).$$

3. If $F_{i-\frac{1}{2}, k} < 0$ and $F_{i+\frac{1}{2}, k} \leq 0$, let

$$\left(\Lambda_{-\frac{1}{2}, I_i, k}^m, \Lambda_{+\frac{1}{2}, I_i, k}^m\right) = \left(\min\left(1, \frac{\Gamma_{i, k}^{m_x}}{\lambda F_{i-\frac{1}{2}, k} - \epsilon}\right), 1\right).$$

4. If $F_{i-\frac{1}{2}, k} < 0$ and $F_{i+\frac{1}{2}, k} > 0$,

- (a) When (4.19) holds with $(\theta_{i-\frac{1}{2}, k}, \theta_{i+\frac{1}{2}, k}) = (1, 1)$, let

$$\left(\Lambda_{-\frac{1}{2}, I_i, k}^m, \Lambda_{+\frac{1}{2}, I_i, k}^m\right) = (1, 1);$$

- (b) Otherwise, let

$$\left(\Lambda_{-\frac{1}{2}, I_i, k}^m, \Lambda_{+\frac{1}{2}, I_i, k}^m\right) = \left(\frac{\Gamma_{i, k}^{m_x}}{\lambda F_{i-\frac{1}{2}, k} - \lambda F_{i+\frac{1}{2}, k} - \epsilon}, \frac{\Gamma_{i, k}^{m_x}}{\lambda F_{i-\frac{1}{2}, k} - \lambda F_{i+\frac{1}{2}, k} - \epsilon}\right).$$

In the above algorithm, we choose ϵ to be a very small positive number to avoid the denominator being 0. For example, we take $\epsilon = 10^{-13}$. Then the locally defined limiting parameter along the x direction is given as

$$\theta_{i+\frac{1}{2}, k} = \min(\Lambda_{+\frac{1}{2}, I_i, k}^m, \Lambda_{-\frac{1}{2}, I_{i+1}, k}^m), \quad i = 0, \dots, N_x. \tag{4.24}$$

Since the process of obtaining the $\left(\Lambda_{I_i, k, -\frac{1}{2}}^m, \Lambda_{I_i, k, +\frac{1}{2}}^m\right)$ is similar to that of $\left(\Lambda_{-\frac{1}{2}, I_i, k}^m, \Lambda_{+\frac{1}{2}, I_i, k}^m\right)$. We also can obtain the limiting parameter along the y direction by the same algorithm

$$\theta_{i, k+\frac{1}{2}} = \min(\Lambda_{I_i, k, +\frac{1}{2}}^m, \Lambda_{I_i, k+1, -\frac{1}{2}}^m), \quad k = 0, \dots, N_y. \tag{4.25}$$

Finally, for r^{n+1} and r_2^{n+1} , we can find the parameters θ and θ_2 following the algorithm given above, respectively. Due to consistency requirement of the numerical fluxes in the equations satisfied by r^{n+1} and r_2^{n+1} , we can choose

$$\tilde{\theta}_{i+\frac{1}{2}, k} = \min\{\theta_{i+\frac{1}{2}, k}, \theta_{2i+\frac{1}{2}, k}\}, \quad \tilde{\theta}_{i, k+\frac{1}{2}} = \min\{\theta_{i, k+\frac{1}{2}}, \theta_{2i, k+\frac{1}{2}}\}$$

as the parameters applied in the scheme (4.16).

Remark 4.7 In the above algorithm, we take $\tilde{\theta}$ to be the smallest one between θ and θ_2 , then we can get positive r^{n+1} and r_2^{n+1} . Then the condition $r^{n+1} + r_2^{n+1} = \phi^{n+1}$ yields $0 \leq r^{n+1} \leq \phi^{n+1}$.

4.3 High-Order Time Discretization

In the previous subsection, all the analysis are based on Euler forward time discretization. For high-order ones, we use the third-order strong-stability-preserving (SSP) time discretization to solve the ODE system $\mathbf{w}_t = \mathbf{L}(\mathbf{w})$:

$$\begin{aligned} \mathbf{w}^{(1)} &= \mathbf{w}^n + \Delta t \mathbf{L}(\mathbf{w}, t^n), \\ \mathbf{w}^{(2)} &= \frac{3}{4} \mathbf{w}^n + \frac{1}{4} \left(\mathbf{w}^{(1)} + \Delta t \mathbf{L}(\mathbf{w}^{(1)}, t^{n+1}) \right), \\ \mathbf{w}^{n+1} &= \frac{1}{3} \mathbf{w}^n + \frac{2}{3} \left(\mathbf{w}^{(2)} + \Delta t \mathbf{L}(\mathbf{w}^{(2)}, t^n + \frac{\Delta t}{2}) \right). \end{aligned}$$

Another choice is the third-order SSP multi-step method:

$$\mathbf{w}^{n+1} = \frac{16}{27} (\mathbf{w}^n + 3 \Delta t \mathbf{L}(\mathbf{w}^n, t^n)) + \frac{11}{27} \left(\mathbf{w}^{n-3} + \frac{12}{11} \Delta t \mathbf{L}(\mathbf{w}^{n-3}, t^{n-3}) \right).$$

More details can be found in [9,10,24]. Since the third-order SSP time discretization is a convex combination of Euler forward time discretization, we can apply the flux limiter designed in Sect. 4.2 to each stage/step to obtain the physically relevant numerical solutions.

5 Numerical Experiments

In this section, some numerical experiments using the the high-order BP FD method have been carried out. In all experiments, we only consider linear weights in the reconstruction procedure. Moreover, we use third-order SSP Runge-Kutta discretization in time and fifth-order finite difference scheme ($r = s = 2$) in space.

Example 5.1 We first test the accuracy of the high-order bound-preserving FD scheme and take $\Omega = [0, 2\pi] \times [0, 2\pi]$. We use periodic boundary condition and take $\mathbf{u} = (1, 1)^T$. The initial condition is given as

$$c_f(x, y, 0) = \sin^4(x + y), \quad \phi(x, y, 0) = 0.5 + 0.4 \sin(x) \sin(y),$$

and the source functions are taken as

$$f_I = 2\phi_t, \quad f_P = \phi_t, \quad c_I = 1.$$

Other parameters are chosen as

$$\mathbf{D} = 0, \quad k_c = k_s = a_0 = \frac{\alpha}{\rho_s} = 1.$$

In the numerical simulation, we choose $N_x = N_y = M$ with $M = 20, 40, 80, 160, 320$, respectively. We take $\Delta t = 0.1h^2$ ($h = \Delta x = \Delta y$) and compute up to $T = 0.01$. Moreover, we use spectral method with fourth-order Runge-Kutta time discretization to obtain the reference solution. The numerical results are given in Table 1, showing the error and convergence order of c_f and ϕ .

Table 1 Example 5.1: Accuracy test for c_f and ϕ with and without bound-preserving technique

M	c_f						ϕ					
	without limiter			with limiter			without limiter			with limiter		
	L^∞ error	Order	Minimum value	L^∞ error	order	Minimum value	L^∞ error	Order	L^∞ error	Order	L^∞ error	Order
20	4.46e-03	-	- 4.22e-03	1.48e-02	-	1.40e-13	8.41e-06	-	4.25e-05	-	4.25e-05	-
40	2.64e-04	4.08	- 1.19e-04	3.97e-04	5.22	2.15e-13	4.62e-07	4.19	1.04e-06	5.36	1.04e-06	5.36
80	1.36e-05	4.28	- 4.81e-06	1.48e-05	4.75	4.76e-11	2.17e-08	4.42	2.49e-08	5.38	2.49e-08	5.38
160	4.71e-07	4.86	- 1.65e-07	4.67e-07	4.99	3.37e-13	7.85e-10	4.79	7.84e-10	4.99	7.84e-10	4.99
320	1.54e-08	4.93	- 5.48e-09	1.54e-08	4.92	3.55e-13	2.56e-11	4.94	2.57e-11	4.93	2.57e-11	4.93

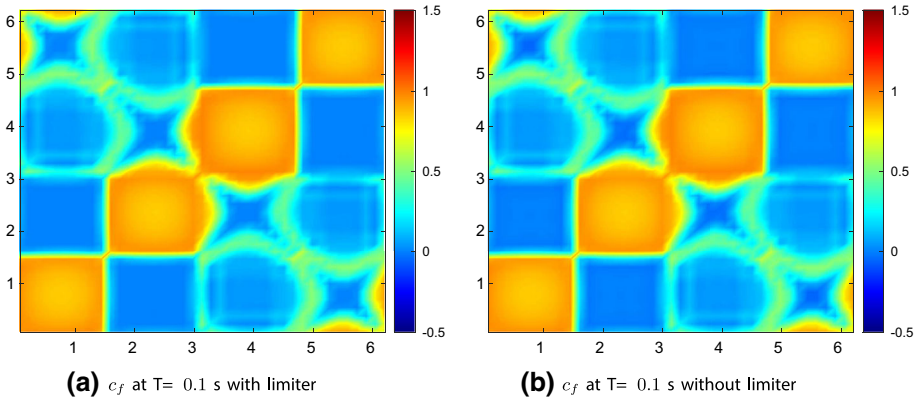


Fig. 1 Example 5.2: Numerical approximations of concentration of acid c_f at $t = 0.1$

From the table, we can observe fifth-order accuracy of the FD scheme with and without the BP limiter. In addition, negative values of c_f appears if the BP technique is not applied, and the parameterized flux limiters remedied the negative values in a conservative way. Therefore, the BP technique does not kill the accuracy when it works.

Example 5.2 We choose the initial conditions with large gradients

$$c_f(x, y, 0) = \frac{\text{sign}(\sin(2x)\sin(2y)) + 1}{2},$$

$$\phi(x, y, 0) = 0.9 \frac{\text{sign}(\sin(x)\sin(y)) + 1}{2} + 0.05.$$

The source functions are chosen as

$$f_I = (1 + \frac{\pi^2}{2} \bar{\phi}_I) \max\{\sin(2x)\sin(2y), 0\}, \quad f_P = -\min\{\sin(2x)\sin(2y), 0\}, \quad c_I = 0,$$

where $\bar{\phi}_I$ is the average of ϕ_I over the whole computational domain. Other parameters are taken as

$$\mu = \kappa_0 = k_c = k_s = \frac{\alpha}{\rho_s} = 1, \quad a_0 = 0.5, \quad \mathbf{D}(\mathbf{u}) = 0.01.$$

We take $N_x = N_y = 41$ over the computational domain $\Omega = [0, 2\pi] \times [0, 2\pi]$. Moreover, we compute up to $T = 0.1$ and choose $\Delta t = 0.2h^2$ ($h = \Delta x = \Delta y$) to reduce the time error. Numerical approximations of c_f with and without BP limiter are given in Fig. 1. We can observe that the numerical simulation with BP limiter is between 0 and 1. To better observe the effect of the BP technique, the distributions of c_f with and without BP limiter at $t = 0.1$ along diagonal $y = 2\pi - x$ are shown in Fig. 2. By using BP technique, all numerical approximations are within the physical bounds.

Example 5.3 We simulate a real wormhole propagation scenario in petroleum engineering to observe the formation and propagation of a wormhole starting from a singular area. The parameters are chosen as

$$\mathbf{D} = 0, \quad \kappa_0 = 10^{-9}m^2, \quad T = 15s,$$

$$\alpha = 100kg/mol, \quad k_c = 1m/s, \quad k_s = 10m/s,$$

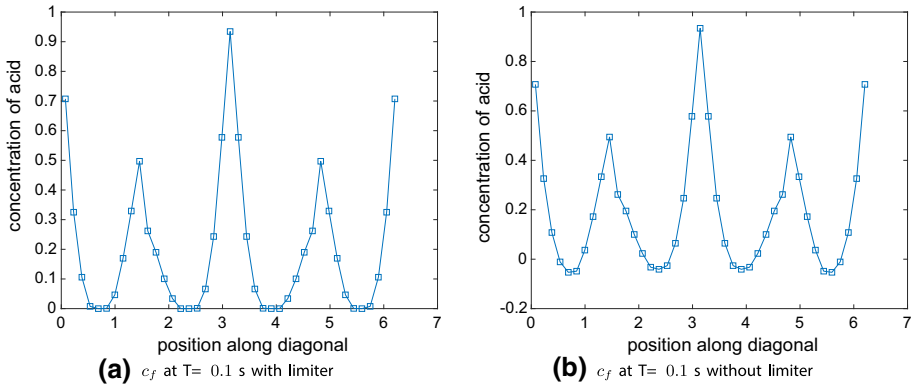


Fig. 2 Example 5.2: Distribution of c_f at $t = 0.1$ along diagonal $y = 2\pi - x$

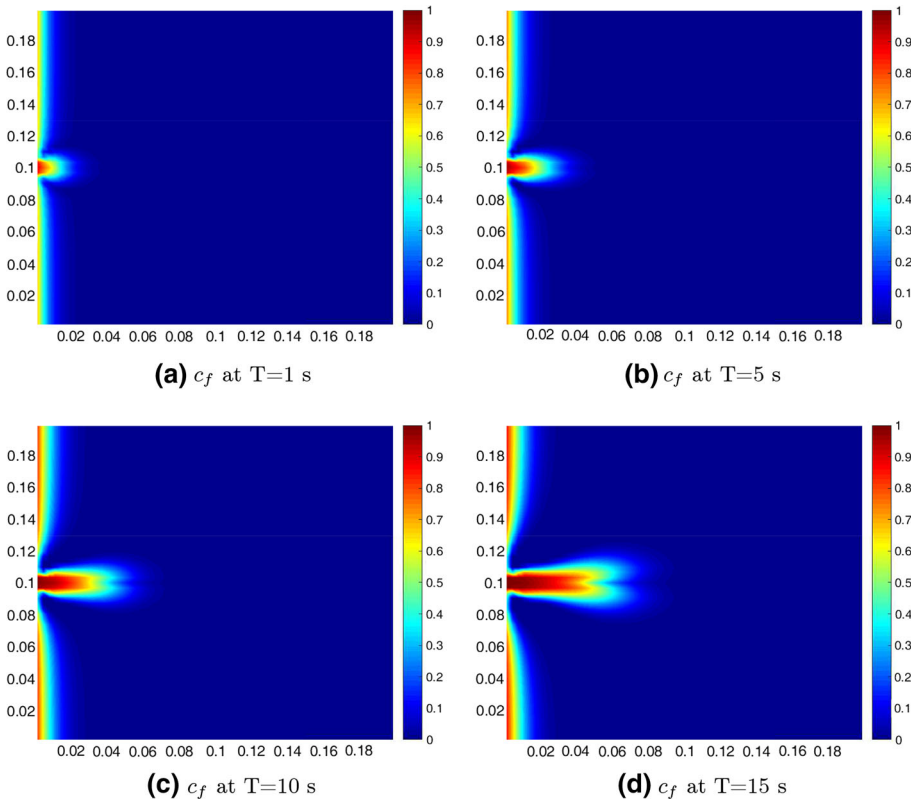


Fig. 3 Example 5.3: Concentration of acid with time evolution

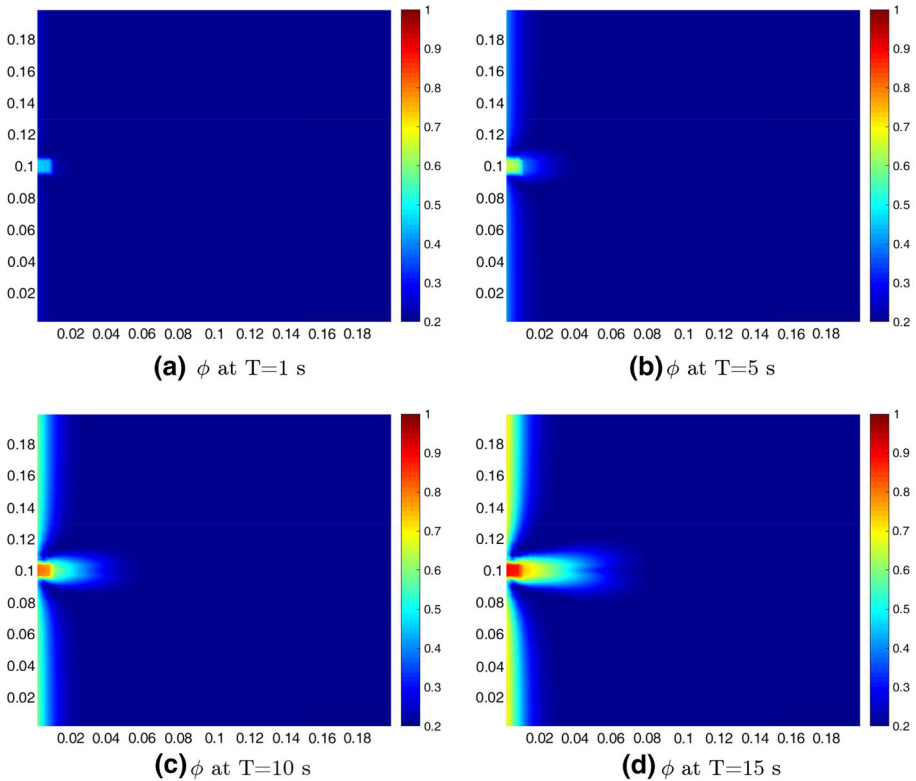


Fig. 4 Example 5.3: Porosity of rock with time evolution

$$\begin{aligned} \mu &= 10^{-2} Pa s, & f_I &= f_P = 0, \\ a_0 &= 2 m^{-1}, & \rho_s &= 2500 kg/m^2. \end{aligned}$$

The computational domain is $\Omega = [0, 0.2 m] \times [0, 0.2 m]$. Initial concentration of acid and initial porosity of rock in this domain are set to be $c_{f0} = 0$ and $\phi_0 = 0.2$, respectively. In order to observe the phenomenon of wormhole propagation, we set a singular area at the middle of the left boundary with size to be $0.01m \times 0.01m$ with high porosity $\phi = 0.4$ and permeability $\kappa = 10^{-8} m^2$. The concentration of influx acid is $1 mol/m^2$ and drained out of it from the right boundary. The upper and lower boundary conditions are set to be periodic. The left and right boundary of the domain are Dirichlet conditions with pressure $p_d = 10000 Pa$ and $p_d = -10000 Pa$, respectively.

The contour plots of the concentration of acid and porosity with time evolution are shown in Figs. 3–4, from which we can observe that the concentration c_f and porosity ϕ are all within their physical bounds.

Example 5.4 To further observe the formation and propagation of wormholes, we set two singular areas with high porosity and permeability on the left boundary with size to be $0.01 m \times 0.01 m$. One is $0.05 m$ above the bottom with porosity 0.4 , and the other is $0.14m$ above the bottom with porosity 0.6 . The permeability of the two entries is determined by

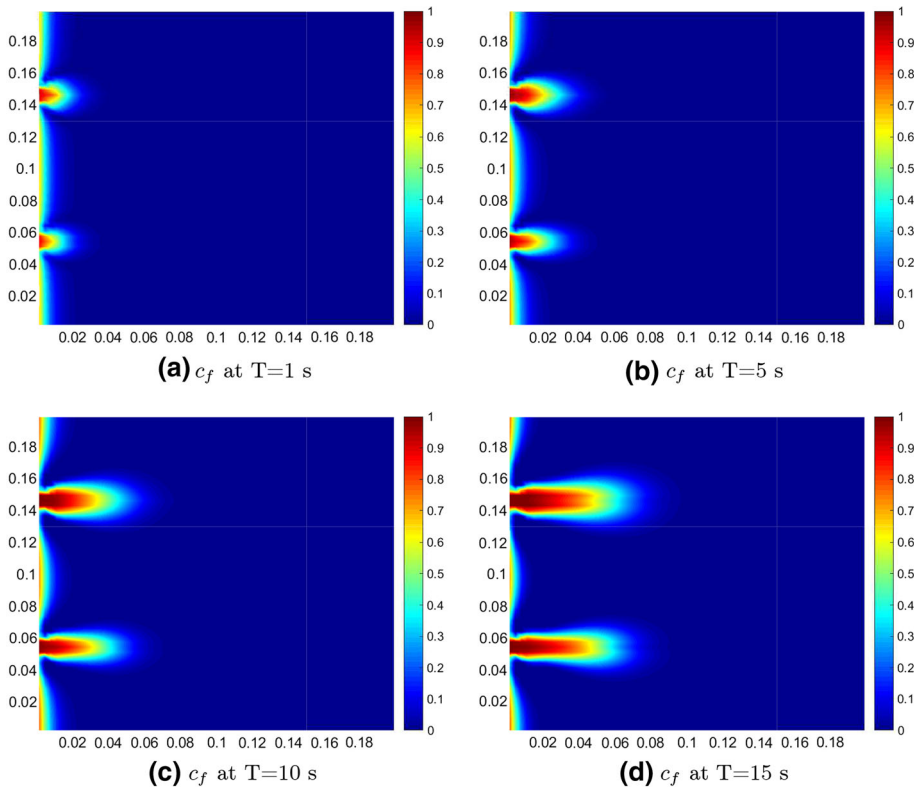


Fig. 5 Example 5.4: Concentration of acid with time evolution

(2.6) which is about $10^{-8} m^2$ and $10^{-7} m^2$, respectively. Other parameters and conditions are the same as in Example 5.3.

The contour plots of the concentration of acid and porosity with time evolution are shown in Figs. 5–6. Wormhole propagation is clearly shown from the figures, and the concentration c_f as well as the porosity ϕ are all within their physical bounds.

6 Concluding Remarks

In this paper, we constructed high-order BP FD methods for incompressible wormhole propagation on rectangular meshes. We have obtained the physically relevant acid concentration and porosity. Numerical simulations have shown the accuracy and good performance of the BP technique.

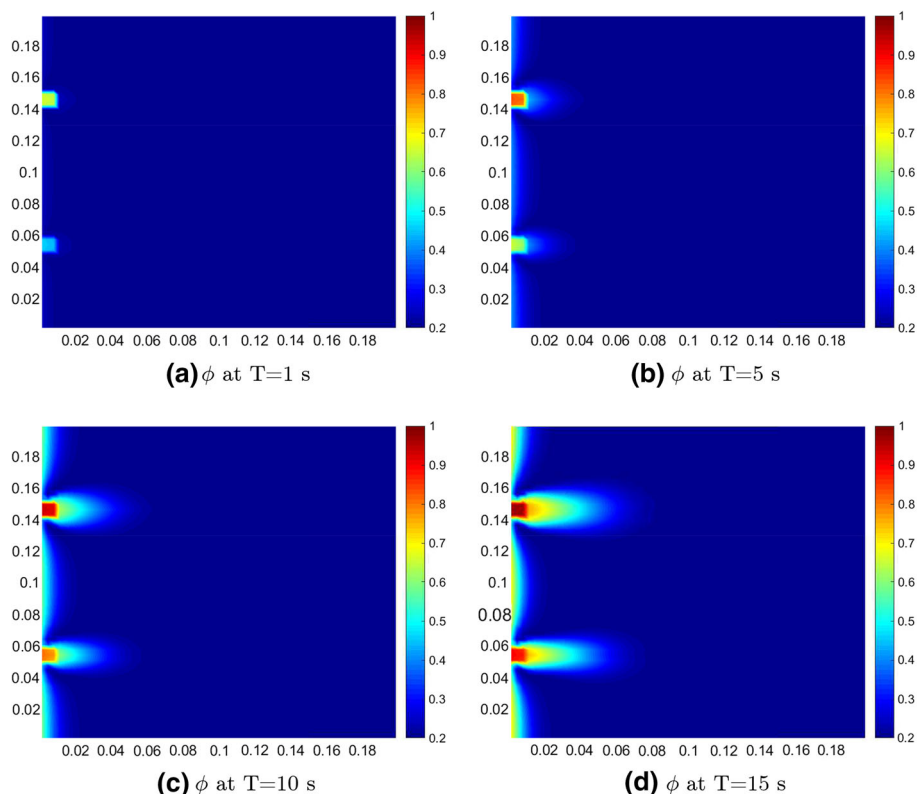


Fig. 6 Example 5.4: Porosity of rock with time evolution

References

1. Akanni, O.O., Nasr-El-Din, H.A., Gusain, D.: A computational Navier-Stokes fluid-dynamics-simulation study of wormhole propagation in carbonate-matrix acidizing and analysis of factors influencing the dissolution process. *SPE J.* **22**, 187962 (2017)
2. Balsara, D.S., Shu, C.-W.: Monotonicity preserving weighted essentially non-oscillatory schemes with increasingly high order of accuracy. *J. Comput. Phys.* **160**, 405–452 (2000)
3. Chuenjarearn, N., Xu, Z., Yang, Y.: High-order bound-preserving discontinuous Galerkin methods for compressible miscible displacements in porous media on triangular meshes. *J. Comput. Phys.* **378**, 110–128 (2019)
4. Douglas, J., Jr., Roberts, J.: Numerical methods for a model for compressible miscible displacement in porous media. *Math. Comput.* **41**, 441–459 (1983)
5. Du, J., Wang, C., Qian, C., Yang, Y.: High-order bound-preserving discontinuous Galerkin methods for stiff multispecies detonation. *SIAM J. Sci. Comput.* **41**, B250–B273 (2019)
6. Du, J., Yang, Y.: Third-order conservative sign-preserving and steady-state-preserving time integrations and applications in stiff multispecies and multireaction detonations. *J. Comput. Phys.* **395**, 489–510 (2019)
7. Fredd, C.N., Fogler, H.S.: Influence of transport and reaction on wormhole formation in porous media. *AIChE J.* **44**, 1933–1949 (1998)
8. Garder, A.O., Jr., Peaceman, D.W., Pozzi, A.L., Jr.: Numerical calculation of multidimensional miscible displacement by the method of characteristics. *Soc. Pet. Eng. J.* **4**, 683 (1964)
9. Gottlieb, S., Ketcheson, D., Shu, C.-W.: High order strong stability preserving time discretizations. *J. Sci. Comput.* **38**, 251–289 (2009)
10. Gottlieb, S., Shu, C.-W., Tadmor, E.: Strong stability-preserving high-order time discretization methods. *SIAM Rev.* **43**(1), 89–112 (2001)

11. Guo, H., Liu, X., Yang, Y.: High-order bound-preserving finite difference methods for miscible displacements in porous media. *J. Comput. Phys.* **406**, 109219 (2020)
12. Guo, H., Tian, L., Xu, Z., et al.: High-order local discontinuous Galerkin method for simulating wormhole propagation. *J. Comput. Appl. Math.* **350**, 247–261 (2019)
13. Guo, H., Yang, Y.: Bound-preserving discontinuous galerkin method for compressible miscible displacement in porous media. *SIAM J. Sci. Comput.* **39**, A1969–A1990 (2017)
14. Hoefner, M.L., Fogler, H.S.: Pore evolution and channel formation during flow and reaction in porous media. *AIChE J.* **34**, 45–54 (1988)
15. Jiang, G., Shu, C.-W.: Efficient implementation of weighted ENO schemes. *J. Comput. Phys.* **126**, 202–228 (1996)
16. Jiang, Y., Xu, Z.: Parametrized maximum principle preserving limiter for finite difference weno schemes solving convection-dominated diffusion equations. *SIAM J. Sci. Comput.* **35**(6), A2524–A2553 (2013)
17. Kou, J., Sun, S., Wu, Y.: Mixed finite element-based fully conservative methods for simulating wormhole propagation. *Comput. Methods Appl. Mech. Eng.* **298**, 279–302 (2016)
18. Li, X., Rui, H.: Characteristic block-centered finite difference method for simulating incompressible wormhole propagation. *Comput. Math. Appl.* **73**, 2171–2190 (2017)
19. Li, X., Rui, H.: Block-centered finite difference method for simulating compressible wormhole propagation. *J. Sci. Comput.* **74**, 1115–1145 (2018)
20. Liu, X.-D., Osher, S., Chan, T.: Weighted essentially nonoscillatory schemes. *J. Comput. Phys.* **115**, 200–212 (1994)
21. Maheshwari, P., Balakotaiah, V.: 3D Simulation of carbonate acidization with HCl: comparison with experiments. In: *SPE Production and Operations Symposium*, Society of Petroleum Engineers (2013)
22. Panga, M.K., Ziauddin, M., Balakotaiah, V.: Two-scale continuum model for simulation of wormholes in carbonate acidization. *AIChE J.* **51**, 3231–3248 (2005)
23. Peaceman, D.W., Rachford, H.H., Jr.: Numerical calculation of multidimensional miscible displacement. *Soc. Pet. Eng. J.* **2**, 471 (1962)
24. Shu, C.-W.: Total-variation-diminishing time discretizations. *SIAM J. Sci. Stat. Comput.* **9**, 1073–1084 (1988)
25. Shu, C.W.: *Essentially Non-Oscillatory and Weighted Essentially Non-Oscillatory Schemes for Hyperbolic Conservation Laws*. Technical Report (1997)
26. Shu, C.-W., Osher, S.: Efficient implementation of essentially non-oscillatory shock-capturing schemes. *J. Comput. Phys.* **77**, 439–471 (1988)
27. Wei, W., Varavei, A., Sepehrnoori, K.: Modeling and analysis on the effect of two-phase flow on wormhole propagation in carbonate acidizing. *SPE J.* **22**, 186111 (2017)
28. Wu, Y., Salama, A., Sun, S.: Parallel simulation of wormhole propagation with the Darcy-Brinkman-Forchheimer framework. *Comput. Geotech.* **69**, 564–577 (2015)
29. Xiong, T., Qiu, J.-M., Xu, Z.: High order maximum-principle-preserving discontinuous Galerkin method for convection-diffusion equations. *SIAM J. Sci. Comput.* **37**, A583–A608 (2015)
30. Xu, Z.: Parametrized maximum principle preserving flux limiters for high order schemes solving hyperbolic conservation laws: one-dimensional scalar problem. *Math. Comput.* **83**, 310–331 (2014)
31. Xu, Z., Yang, Y., Guo, H.: High-order bound-preserving discontinuous Galerkin methods for wormhole propagation on triangular meshes. *J. Comput. Phys.* **390**, 323–341 (2019)
32. Yu, F., Guo, H., Chuenjarern, N., Yang, Y.: Conservative local discontinuous Galerkin method for compressible miscible displacements in porous media. *J. Sci. Comput.* **73**, 1249–1275 (2017)
33. Zhao, C., Hobbs, B.E., Hornby, P., et al.: Theoretical and numerical analyses of chemical-dissolution front instability in fluid-saturated porous rocks. *Int. J. Numer. Anal. Meth. Geomech.* **32**, 1107–1130 (2008)